Valence-band coupling and Fano-resonance effects on the excitonic spectrum in undoped quantum wells

D. A. Broido* and L. J. Sham
Department of Physics, University of California, San Diego, La Jolla, California 92093
(Received 13 May 1986)

An investigation is made of the effects of the valence-band coupling on the excitonic spectrum of undoped GaAs-$Al_xGa_{1-x}As$ quantum wells. The electron and hole are taken to interact via a screened Coulomb attraction, and their respective subbands are determined in the effective-mass approximation. The binding energy of the lowest heavy-hole exciton, E_{0h}^{ex}, is found to increase only slightly. That of the lowest light-hole exciton, E_{0l}^{ex}, shows a more substantial increase because the light-hole exciton derives from a strongly nonparabolic hole subband and, in addition, exhibits a Fano-like resonance with the electron—heavy-hole continuum.

I. INTRODUCTION

Excitonic peaks associated with the so-called light- and heavy-hole excitons—excitons formed from an electron deriving from the lowest conduction ($0c$) subband and a hole deriving from the topmost heavy ($0h$) or light ($0l$) hole subband—characterize the onset of absorption and luminescence in the undoped quantum well.[1] The location of these peaks below their respective continuums specifies the binding energies of the excitons, E_{0h}^{ex} and E_{0l}^{ex}.

In both two and three dimensions, the binding energy of an exciton deriving from parabolic electron and hole bands is directly proportional to the reduced electron-hole mass. Qualitatively, then, in the quasi-two-dimensional case of the quantum well, we expect E_{0h}^{ex} and E_{0l}^{ex} to go like their respective in-plane (i.e., in the plane of the well) reduced electron-hole masses.

Previous calculations of the exciton binding energies[2–4] approximate the hole subbands by parabolas. This approximation neglects the effects of the strong valence-band coupling which results because of the degeneracy of the bulk light- and heavy-hole bands at the valence-band edge. The valence-band coupling mixes the light- and heavy-hole states away from $k=0$, where k is the wave vector in the plane of the well. This mixing gives rise to large nonparabolicities in the hole subband structure which change the effective in-plane hole masses and so alter the binding energies. In addition, the discrete light-hole exciton states lie in the heavy-hole continuum giving rise to Fano-like resonances[5,6] in which the exciton peak is broadened and shifted in energy. This induces a further shift E_{0l}^{ex}.

In this paper we study the significance of these effects on E_{0h}^{ex} and E_{0l}^{ex}. In Sec. II the electron and hole subband structure is calculated including the effect of the valence-band coupling on the hole subbands. In Sec. III a method is developed for determining E_{0h}^{ex} and E_{0l}^{ex} using the subbands derived in Sec. II, and the effect of the valence-band coupling on these quantities is examined. In Sec. IV the absorption spectrum is derived to extract the Fano-like shift in the exciton line associated with E_{0l}^{ex}. Section V presents a discussion of the results and a comparison with the available experimental data.

II. SUBBAND STRUCTURE

The GaAs-$Al_xGa_{1-x}As$ quantum-well consists of a layer of undoped GaAs of width L sandwiched between two semi-infinite slabs of $Al_xGa_{1-x}As$. If we choose the z direction to be normal to the GaAs and $Al_xGa_{1-x}As$ layers, the potentials, $V_e(z_e)$ and $V_h(z_h)$, seen by electrons and holes, respectively, have the simple form

$$V_e(z_e)=\begin{cases}0, & |z_e|<L/2\\ \Delta E_c, & |z_e|>L/2\end{cases}$$
$$V_h(z_h)=\begin{cases}0, & |z_h|<L/2\\ \Delta E_v, & |z_h|>L/2\end{cases}. \tag{1}$$

ΔE_c and ΔE_v are the conduction- and valence-band discontinuities. In this paper we consider both the previously accepted rule[1] $\Delta E_c=0.85\Delta E_g$, $\Delta E_v=0.15\Delta E_g$ (15%-85% split), and the more recently established[7] $\Delta E_v=0.40\Delta E_g$, $\Delta E_c=0.60\Delta E_g$ (40%-60% split), where ΔE_g is the energy-gap discontinuity between the GaAs and $Al_xGa_{1-x}As$. The electron and hole subbands are calculated using the effective-mass approximation. The electron subbands are taken to be uncoupled from the hole subbands and so are parabolic. The electron wave function is

$$\psi_{nk}^{\sigma}=e^{i\mathbf{k}\cdot\rho}\xi_n(z)u^{\sigma}. \tag{2}$$

Here n is the subband index, $\mathbf{k}$ is the in-plane wave vector, and σ designates the spin state of the Bloch function u^{σ}. The envelope functions $\xi_n(z)$ satisfy

$$\left[-\frac{1}{2m}\frac{d^2}{dz^2}+V(z)\right]\xi_n=\varepsilon_n\xi_n \tag{3}$$

and so have the standard finite square-well form. The mass, $m=m_e=0.0065m_0$ in the GaAs, and $m=m_e(x)=m_e+(0.083x)m_0$ in the $Al_xGa_{1-x}As$.[8]

At the left and right interfaces ($z=\pm L/2$), continuity of the wave function and current conservation can be shown to reduce to continuity of ξ_n and $(1/m)(d\xi_n/dz)$. These boundary conditions[9] determine ε_n and ξ_n. The in-plane dispersion is given by

$$\varepsilon_n(k)=\varepsilon_n+\frac{k^2}{2m_e} . \tag{4}$$

Because of the fourfold degeneracy of the bulk light- and heavy-hole bands, the hole subbands are determined from the effective Hamiltonian made up of the 4×4 $\mathbf{k}\cdot\mathbf{p}$ Hamiltonian of Luttinger[10] with the potential $V_h(z)$ included along the diagonal. It is convenient to transform this Hamiltonian into two 2×2 blocks.[11] The hole wave functions then taken the form

$$\psi^{\sigma}_{mk}=e^{i\mathbf{k}\cdot\rho}\sum_{j=h,l}\zeta_{mkj}v^{\sigma}_{j} . \tag{5}$$

Here m is shorthand for (ν,ι), where ν ranks the subband (i.e.,$=0,1,2,\ldots$), and ι characterizes the nature of each subband as one of two heavy-hole (h,σ) or light-hole (l,σ) solutions; σ specifies the upper $(\sigma=U)$ and lower $(\sigma=L)$ block. The v^{σ}_{j} are linear combinations of the $J=\frac{3}{2}$ quadruplet consisting of the valence-band-edge Bloch states.

The effective-mass equations for $\sigma=U,L$ are

$$\begin{bmatrix} H_{hh}-E & H^{\sigma}_{hl} \\ H^{\sigma}_{lh} & H_{ll}-E \end{bmatrix}\begin{bmatrix}\zeta_{mkh}\\ \zeta_{mkl}\end{bmatrix}=0 ,$$

$$H_{jj}=-\frac{1}{2m_{jz}}\frac{d^2}{dz^2}-\frac{k^2}{2m_{j\|}}-V_h(z) , \tag{6a}$$

$$\frac{m_0}{m_{jz}}=\begin{cases}\gamma_1-2\gamma_2, & j=h\\ \gamma_1+2\gamma_2, & j=l\end{cases}$$

$$\frac{m_0}{m_{j\|}}=\begin{cases}\gamma_1+\gamma_2, & j=h\\ \gamma_1-\gamma_2, & j=l\end{cases}$$

$$H^{U}_{hl}=H^{L}_{lh}=-\frac{\sqrt{3}}{2}\bar{\gamma}k^2+\sqrt{3}\gamma_3 k\frac{d}{dz} ,$$

$$H^{U}_{lh}=H^{L}_{hl}=-\frac{\sqrt{3}}{2}\bar{\gamma}k^2-\sqrt{3}\gamma_3 k\frac{d}{dz} , \tag{6b}$$

$$k^2=k_x^2+k_y^2,\ \bar{\gamma}=\tfrac{1}{2}(\gamma_2+\gamma_3) .$$

The band-structure parameters, $\gamma_1=6.85$, $\gamma_2=2.1$, and $\gamma_3=2.9$, are taken from Ref. 12.

In these equations terms producing subband anisotropy, e.g., anisotropy in the in-plane dispersion, have been neglected so that the energy depends only on $k=|\mathbf{k}|$.[11,13] The hole subband structure is determined using the subband $\mathbf{k}\cdot\mathbf{p}$ method.[11,13] First, k is taken to be zero, for which the light- and heavy-hole states decouple (i.e., the above Hamiltonian becomes diagonal). The diagonal elements then generate equations which have the same form as Eq. (3) with the replacement $V_e\rightarrow V_h$, and the appropriate insertions for the heavy- and light-hole masses in the z direction [i.e., m_{hz} and m_{lz} in the GaAs, $m_{hz}(x)=m_{hz}+(0.31x)m_0$, $m_{lz}(x)=m_{lz}+(0.049x)m_0$ in the $Al_xGa_{1-x}As$ (Ref. 8). The solutions, which we denote by $\psi_{\nu j}$ $(\nu=0,1,2,\ldots,\ j=h,l)$, have the same functional form as the ξ_n.

For finite k, the envelope functions (ζ_{mkj}) are expanded using the $(\psi_{\nu j})$ as a basis

$$\zeta_{mkj}=\sum_{\nu_j}A_{m\nu_j j}(k)\psi_{\nu_j j} \tag{7}$$

where ν_j runs over the confined levels of type $j=h$ and $j=l$. The eigenvalue matrix for the coefficients $A_{m\nu_j j}(k)$ is then diagonalized to obtain the subband structure.

Because of the complicated nature of the numerical solution for the binding energies, only the top two heavy-hole $(0h,1h)$ and light-hole $(0l,1l)$ levels are retained in the expansion. We will refer to this model for the subbands as the four-level model. It should provide an accu-

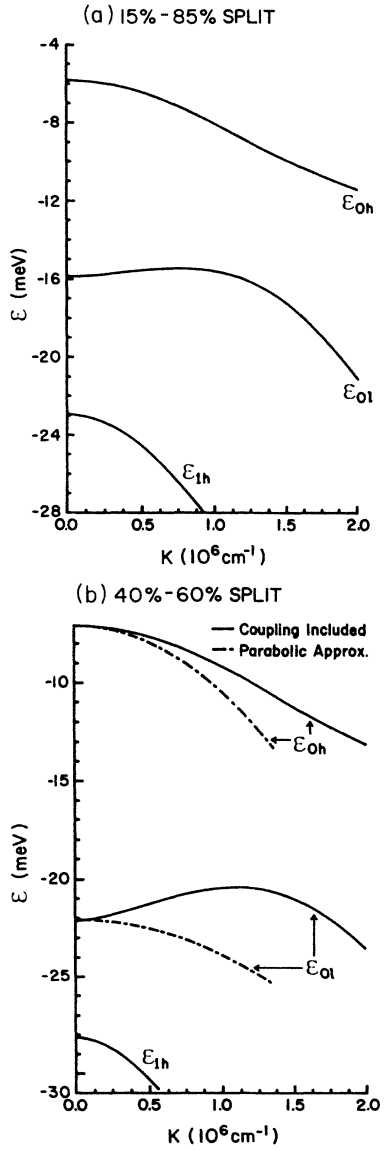

FIG. 1. (a) Topmost three-hole subbands for the 15%-85% split. (b) Topmost three subbands for the 40%-60% split. Dashed curves are for the parabolic approximation.

rate representation of the topmost two subbands for well widths small enough that sufficiently large energy-level spacings occur. An example of such a case is the 100-Å well with $x=0.3$, for which the $0h$ and $0l$ subbands determined in the four-level model differ negligibly from those determined using the full subband $\mathbf{k}\cdot\mathbf{p}$ matrix. The topmost three subbands for a 100-Å well with $x=0.3$ are shown in Fig. 1 for the 15%-85% and 40%-60% splits. The dashed lines in Fig. 1(b) represent the parabolic approximation. The inclusion of the valence-band coupling introduces an anticrossing behavior between the light- and heavy-hole subbands which flattens the topmost two subbands ($0h$ and $0l$), and "steepens" the first excited ($1h$) heavy-hole subband. The nonparabolicity in the $0l$ subband is considerably larger than that in the $0h$ subband because of the mutual repulsion of the $0l$ and $1h$ subbands arising from the small energy separation between them. We therefore expect $E_{0l}^{\rm ex}$ to show a larger increase than $E_{0h}^{\rm ex}$ when valence-band coupling is included. The subbands for the 15%-85% split exhibit a similar form except the $0l$ subband does not show as sharp an electronlike curvature since the $0l$ and $1h$ subbands are not as close.

III. DETERMINATION OF THE BINDING ENERGIES

We begin by defining the exciton as an excited state of the many-particle system. In the weak binding (Wannier) limit, the exciton motion can be described by an effective Hamiltonian for the quasielectron and quasihole bound by a screened Coulomb attraction.[14] We consider only conduction and valence subbands, so that this Hamiltonian can be written

$$\hat{H}=\hat{H}_e+\hat{H}_h+\hat{U} \ . \tag{8}$$

The electron and hole parts $\hat{H}_e$ and $\hat{H}_h$ are given by

$$\hat{H}_e=\sum_{\lambda_e}\varepsilon_{\lambda_e}c_{\lambda_e}^{\dagger}c_{\lambda_c} \ , \tag{9}$$

$$\hat{H}_h=\sum_{\lambda_h}\varepsilon_{\lambda_h}b_{\lambda_h}^{\dagger}b_{\lambda_h} \ .$$

Here $c_{\lambda_e}^{\dagger}$ and c_{λ_e} are the creation and destruction operators for electrons in the state $\lambda_e=n,\mathbf{k}_e,\sigma_e$, while $b_{\lambda_h}^{\dagger}$ and b_{λ_h} are the creation and destruction operators for holes in the state $\lambda_h=m\,\mathbf{k}_h\sigma_h$. ε_{λ_e} and ε_{λ_h} are the corresponding subband energies. The interaction between the electron and hole is the screened Coulomb attraction,

$$\hat{u}=\sum_{\lambda_e'\lambda_h'}\langle\lambda_e\lambda_h\,|\,u\,|\,\lambda_e'\lambda_h'\rangle c_{\lambda_e}^{\dagger}c_{\lambda_e'}b_{\lambda_h}^{\dagger}b_{\lambda_h'} \ , \tag{10}$$

$$u=\frac{-e^2}{\epsilon\,|\,\mathbf{r}_e-\mathbf{r}_h\,|} \ ,$$

where ϵ is the GaAs dielectric constant.

We consider a single electron-hole pair and look for solutions of

$$\hat{H}\,|\,\Psi\rangle=E\,|\,\Psi\rangle \ , \tag{11}$$

where $|\,\Psi\rangle$ is the excited-state wave function. We expand in terms of products of the electron and hole effective-mass wave functions of Sec. II,

$$|\,\Psi\rangle=\sum_{\lambda_e,\lambda_h}\Phi_{\lambda_h}^{\lambda_e}c_{\lambda_e}^{\dagger}b_{\lambda}^{\dagger}\,|\,0\rangle \ , \tag{12}$$

where $|\,0\rangle$ is the ground state (filled valence subbands, empty conduction subbands). Projecting onto a particular state, $c_{\lambda_e}^{\dagger}b_{\lambda_h}^{\dagger}\,|\,0\rangle$, yields

$$(\varepsilon_{\lambda_e}+\varepsilon_{\lambda_h}-E)\Phi_{\lambda_h}^{\lambda_e}+\sum_{\lambda_e',\lambda_h'}\langle\lambda_e\lambda_h\,|\,u\,|\,\lambda_e'\lambda_h'\rangle\Phi_{\lambda_h'}^{\lambda_e'}=0 \ . \tag{13}$$

The Coulomb interaction is treated as slowly varying, and orthogonality of the Bloch functions then requires that the matrix element be diagonal in the spin indices. We express u as a two-dimensional Fourier expansion.[15] Then, because the total in-plane momentum is conserved, we make the transformation, $\mathbf{k}_e=\frac{1}{2}\mathbf{K}+\mathbf{k}$, $\mathbf{k}_h=\frac{1}{2}\mathbf{K}-\mathbf{k}$, and neglect the translational motion so that $\mathbf{K}=\mathbf{0}$. Treating $\mathbf{k}$ as a continuous variable and using the subband $\mathbf{k}\cdot\mathbf{p}$ expansion for the hole envelope functions, we obtain

$$[\varepsilon_n(k)-\varepsilon_m(k)-E]\Phi_m^n(k)+\sum_{n',m'}\int V_{mm'}^{nn'}(k,k')\Phi_{m'}^{n'}(k')dk'=0 \ ,$$

$$V_{mm'}^{nn'}(k,k')=k'\sum_{\nu_j,\nu_j'}A_{m\nu_j j}^{*}(k)A_{m'\nu_j' j}(k')\times\int_0^{2\pi}V(q)I_{\nu_j\nu_j'}^{nn'}(q)d\theta \ , \tag{14}$$

where

$$I_{\nu_j\nu_j'}^{nn'}(q)=\int_{-\infty}^{\infty}\int_{-\infty}^{\infty}\xi_n^{*}\xi_{n'}\psi_{\nu_j j}^{*}\psi_{\nu_j' j}e^{-q\,|\,z_e-z_h\,|}\,dz_e\,dz_h \ , \tag{15}$$

$$V(q)=-\frac{2\pi e^2}{\epsilon q}, \quad q=|\,\mathbf{k}-\mathbf{k}'\,| \ .$$

In the above expression, the angular dependence in $\Phi_m^n(k)$ has been removed by considering only the s-like exciton states.

To determine $V_{mm'}^{nn'}(k,k')$, the four-level model is employed. The double integral $I_{\nu_j\nu_j'}^{nn'}(q)$, is time consuming to evaluate numerically. We instead take the infinite-well wave functions, which simplifies the analytic expressions considerably. The finite square well width L is replaced by larger infinite well widths $L_{\rm eff}$ to compensate for the fact that the infinite-well wave functions vanish at the interfaces. These widths are chosen to accurately model the exact $I_{\nu_j\nu_j'}^{nn'}(q)$ and correspond roughly to well widths for which the energy level of the infinite well matches that of the finite well.

We are interested in the lowest heavy-hole and light-hole excitons corresponding to the two cases ($n=0c,m=0h$) and ($n=0c,m=0l$). For well widths small enough that the difference in energy between an electron-hole pair associated with the excited subbands ($n'm'$) and one associated with the ground subbands [($0c,0h$) or ($0c,0l$)] is large compared to the binding ener-

gies (≈ 10 meV), the expansion coefficients Φ_{0h} and Φ_{0l} are much larger than the other components, and we neglect the latter. The exciton wave function is then

$$|\Psi\rangle = \sum_{\mathbf{k}} [\Phi_{0h}^{0c}(k) C_{0ck\sigma_e}^{\dagger} b_{0hk\sigma_h}^{\dagger} + \Phi_{0l}^{0c}(k) c_{0ck\sigma_e}^{\dagger} b_{0lk\sigma_h}^{\dagger}] |0\rangle . \quad (16)$$

The form of this wave function shows that the electron—heavy-hole $0c$-$0h$ states and electron—light-hole $0c$-$0l$ states are mixed, i.e., scattering between $0c$-$0h$ states and $0c$-$0l$ states can occur. We refer to the interaction that mixes these states as the intersubband interaction. The resulting pair of coupled integral equations is

$$[\varepsilon_{0c}(k) - \varepsilon_m(k) - E]\Phi_m(k) + \sum_{m'=0h,0l} \int V_{mm'}(k,k')\Phi_{m'}(k')dk' = 0 . \quad (17)$$

These equations contain a logarithmic singularity in the kernel $V_{mm'}$ at $q=0$ because $V(q) \propto 1/q$. The modified quadrature method[16] is particularly suited for solving integral equations with this type of singularity, and we use it to solve Eq. (17).

Solutions are obtained in three successively improved approximations:

(1) Valence-band coupling and intersubband interaction neglected (parabolic approximation).

(2) Valence-band coupling included; intersubband interaction neglected.

(3) Both valence-band coupling and intersubband interaction included.

For approximations (1) and (2), the integral equations of Eq. (17) decouple since the $0c$-$0h$ states and the $0c$-$0l$ states are now assumed not to mix.

Figure 2 displays E_{0h}^{ex} and E_{0l}^{ex} as a function of well width for the 15%-85% and 40%-60% splits. The decrease in binding energy with increasing well width reflects the increase in the spatial extent of the exciton along the quantum-well axis. Note that as L decreases, the increase in E_{0l}^{ex} is greater than for E_{0h}^{ex}, a consequence of the strong nonparabolicities in $\varepsilon_{0l}(k)$ shown in Fig. 1. The corresponding increase for the case of the 15%-85% split is smaller because $\varepsilon_{0l}(k)$ is not as nonparabolic. The crossing of the E_{0l}^{ex} curves for the 15%-85% split at $L \approx 250$ Å reflects the inadequacy of the four-level model for this large a well width. Were more levels retained, the $0l$ subband would become flatter and E_{0l}^{ex} would increase.

One might expect that with the electronlike curvature of the $0l$ subband, the increase in E_{0l}^{ex} would be much larger. The reason this is not so can be understood by examining Fig. 3 which shows the reduced mass μ as a function of effective hole mass m. The vertical lines indicate the heavy- and light-hole in-plane masses, $m_{h_{||}}$ and $m_{l_{||}}$, in the parabolic approximation. The heavy-hole subband is not altered significantly with the inclusion of valence-band coupling, so one would expect only a small increase in the effective heavy-hole mass with a correspondingly small increase in μ. For the strongly nonparabolic light-hole subband, a large increase in effective mass is expected. However, since the curve is quite flat for $m > m_{l_{||}}$ even a large increase in m produces only a small increase in μ. We conclude from this that the exciton binding energies, particularly that of the light-hole exci-

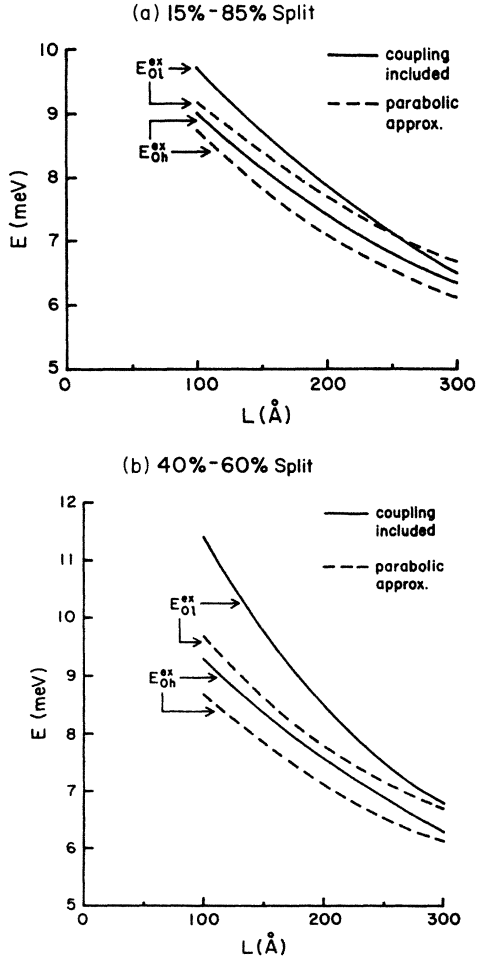

FIG. 2. Exciton binding energies vs well width with and without valence-band coupling for (a) the 15%-85% split and (b) the 40%-60% split.

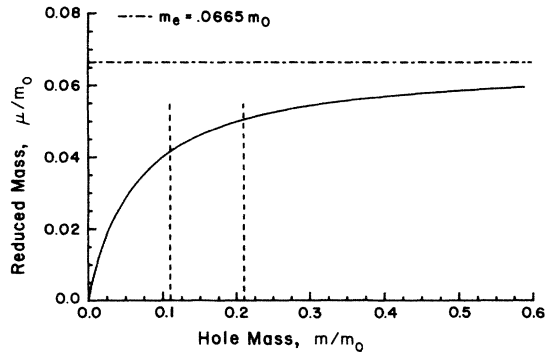

FIG. 3. Reduced electron-hole mass vs effective hole mass.

ton, do not depend sensitively on the nonparabolicities in the hole subbands because the reduced mass is dominated by the electron mass.

IV. ABSORPTION SPECTRUM FOR THE UNDOPED QUANTUM WELL

If we examine the joint density of states, it is evident that the light-hole exciton lies in the $0c$-$0h$ continuum. When the intersubband interaction is turned on [approximation (3)], this exciton decays leading to a resonance that is shifted in energy.[5,6]

Since the $0c$-$0h$ and $0c$-$0l$ states are now mixed, we can no longer identify a single eigenvalue corresponding to $E_{0l}^{\rm ex}$. Instead we calculate the absorption spectrum in the absence and in the presence of the intersubband interaction. The desired energy shift is extracted from the difference in the location of the respective exciton peaks.

We wish to calculate the absorption spectrum for radiation of frequency ω along the quantum-well axis. Absorption in a crystal is characterized by the imaginary part of the dielectric function, $\epsilon_2(\omega)$, which can be broken into two components:

$$\epsilon_2(\omega)=\epsilon_2^{\rm ex}(\omega)+\epsilon_2^{\rm con}(\omega)\ . \tag{18}$$

The first term represents the excitonic contribution to the absorption while the second represents that from the continuum. Let us first neglect the intersubband scattering [approximation (2)]. Utilizing the excited-state wave functions of Sec. III and employing the dipole approximation, we obtain

$$\begin{aligned}\epsilon_2^{\rm ex}(\omega)&=\frac{8\pi^2e^2}{m_0^2\omega^2}\sum_{m,a,\sigma_e,\sigma_h}\left|\sum_{k'}\Phi_{m,a}(k')\langle\psi_{nk'}^{\sigma_e}|\hat{\varepsilon}\cdot\mathbf{p}|\psi_{mk'}^{\sigma_h}\rangle\right|^2\delta(E_{m,a}-E_0-\omega)\ ,\\ \epsilon_2^{\rm con}(\omega)&=\frac{8\pi^2e^2}{m_0^2\omega^2}\sum_{m,k,\sigma_e,\sigma_h}\left|\sum_{k'}\Phi_{m,k}(k')\langle\psi_{nk'}^{\sigma_e}|\hat{\varepsilon}\cdot\mathbf{p}|\psi_{mk'}^{\sigma_h}\rangle\right|^2\delta(\varepsilon_{0c}(k)-\varepsilon_m(k)-\omega)\ .\end{aligned} \tag{19}$$

Here $\mathbf{p}$ is the single-particle momentum operator, and $\hat{\varepsilon}$ is the polarization vector of the incident light which is taken to be right-circularly polarized so that $\Delta m_j=1$ transitions are induced (no loss of generality occurs here since the double degeneracy of the subbands means that left-circularly polarized light produces the same absorption spectrum). The eigenvalues, $E_{m,a}-E_0$ and $\varepsilon_{0c}(k)-\varepsilon_m(k)$, and eigenvectors $\Phi_{m,a}(k')$ and $\Phi_{m,k}(k')$, are determined by solving the integral equations, Eq. (14), and taking $m=m'$ [approximation (2)]. The subscript a labels the exciton state, e.g., $1s$, $2s$, etc., while k specifies the energy of the continuum states.

Using the subband $\mathbf{k}\cdot\mathbf{p}$ expansion, $\epsilon_2^{\rm ex}(\omega)$ and $\epsilon_2^{\rm con}(\omega)$ can be rewritten as

$$\begin{aligned}\epsilon_2^{\rm ex}(\omega)&=\frac{4\pi^2e^2}{m_0\omega}\sum_{m,a}f_{m,a}\delta(E_{m,a}-E_0-\omega)\ ,\\ \epsilon_2^{\rm con}(\omega)&=\frac{4\pi^2e^2}{m_0\omega}\sum_{m,k}f_{m,k}\delta(\varepsilon_{0c}(k)-\varepsilon_m(k)-\omega)\ ,\end{aligned} \tag{20}$$

where $f_{m,a}$ and $f_{m,k}$ are oscillator strengths for the excitonic and continuum states, respectively,

$$\begin{aligned}f_{m,a}&=\frac{2p^2}{m_0\omega}[(I_{mh}^aS_{0h})^2+\tfrac{1}{3}(I_{ml}^aS_{0l})^2]\ ,\\ I_{mj}^a&=\sum_{k'}\Phi_{m,a}(k')A_{m0j}(k')\ ,\\ S_{0j}&=\int_{-\infty}^{\infty}\xi_{0c}\psi_{0j}\,dz\ ,\end{aligned} \tag{21}$$

with similar expressions for $f_{m,k}$. Here p is the momentum matrix element $\langle s\,|\,p_x\,|\,x\rangle$ and the factor of $\frac{1}{3}$ in the second term inside the square brackets arises from the momentum matrix element between conduction- and light-hole band-edge Bloch states. In the absence of valence-band coupling [$A_{m0j}(k)=\delta_{m,0j}$], the relative transition strengths for heavy and light holes, f_{0h}/f_{0l}, become 3 to 1 when $s_{0h}=s_{0l}$. To evaluate these expressions, the δ functions are replaced with Lorentzians of half-width Γ. The value of Γ is difficult to calculate, and since we are interested only in the location of the exciton peaks, it does not have to be accurately determined. Values of $\Gamma_{\rm ex}=1$ meV and $\Gamma_{\rm con}=2$ meV are chosen to give sharp exciton peaks and a smooth continuum. $\epsilon_2(\omega)$ for the 100-Å well with $x=0.3$ (taking the 40%-60% split) is plotted in Fig. 4. The onset of the $0c$-$0h$ and $0c$-$0l$ continuums are marked along the horizontal axis. Observe that the light-hole exciton lies in the $0c$-$0h$ continuum.

TABLE I. Exciton binding energies for $L=100$ Å and $x=0.3$. The labels 1, 2, and 3 refer to approximations (1), (2), and (3) as defined in Sec. III.

	$E_{0h}^{\rm ex}$ (meV)			$E_{0l}^{\rm ex}$ (meV)		
Split	1	2	3	1	2	3
15%-85%	8.8	9.0	9.3	9.3	9.7	10.5
40%-60%	8.7	9.3	9.5	9.7	11.4	12.6

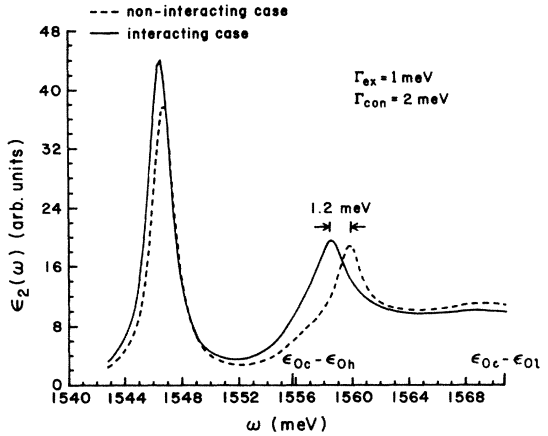

FIG. 4. Calculated absorption spectrum with (solid line) and without (dashed line) the intersubband interaction.

With the intersubband interaction turned on, the coupling terms $m \neq m'$ must be included in the solution of Eq. (17), and additional terms enter into the oscillator strengths which arise from the mixing of the $0c$-$0h$ and $0c$-$0l$ states. These terms produce shifts in the locations of the exciton peaks, as shown by the solid line of Fig. 4. A slight shift of ≈ 0.2 meV occurs for the heavy-hole peak, while a more noticeable shift of ≈ 1.2 meV occurs for the light-hole peak.

V. DISCUSSION AND CONCLUSIONS

The values of E_{0h}^{ex} and E_{0l}^{ex} for approximations (1), (2), and (3) are give in Table I for the 100-Å well, $x=0.3$. These results reflect the following conclusions about the significance of the valence-band coupling and intersubband interaction. With the inclusion of valence-band coupling:

(1) E_{0h}^{ex} and E_{0l}^{ex} increase with the larger increase occurring for E_{0l}^{ex} because the $0l$ subband becomes substantially more nonparabolic than does the $0h$ subband (Fig. 1).

(2) The increase in E_{0l}^{ex} is larger for the 40%-60% split than for the 15%-85% split because the $0l$ subband for the former case exhibits a sharper electronlike curvature and so has associated with it a larger effective mass.

TABLE II. Calculated energy difference between the $1s$ and $2s$ excitons compared with experiment.

Split	$E_{0h}^{1s\text{-}2s}$ (meV)	$E_{0l}^{1s\text{-}2s}$ (meV)
15%-85%	7.5	7.7
40%-60%	7.6	8.7
Expt.[2]	7.6	8.7

(3) The increase in binding is smaller than might be expected (particularly given the strongly nonparabolic $0l$ subband) because the reduced mass is dominated by the electron mass.

With the inclusion of the intersubband interaction:

(1) The binding energies increase further. Again, the increase is largest for E_{0l}^{ex} because it is immersed in the $0c$-$0h$ continuum and so exhibits a Fano-like resonance.

(2) The shift in E_{0l}^{ex} is again larger for the 40%-60% split than for the 15%-85% split because for the latter case, E_{0l}^{ex} lies just at the onset of the $0c$-$0h$ edge and so does not interact as strongly with the continuum states.

Comparison of the results of the present calculation with experiment is hindered by the fact that determination of the exciton binding energies is difficult to obtain experimentally. Photoexcitation measurements, in particular, suffer from an inability to accurately resolve the onset of the continuum transitions. A comparison can be made, though, with the results of Miller *et al.*,[2] who directly measure the difference in the binding energies of the $1s$ and $2s$ excitons, $E_{0h}^{1s\text{-}2s}$ and $E_{0l}^{1s\text{-}2s}$. Table II displays the theoretical and experimental values for a 100-Å well with $x=0.37$. The value of $E_{ol}^{1s\text{-}2s}$ obtained for the 15%-85% split is too small compared with experiment because E_{0l}^{ex} itself is too small for this case. The agreement between the theory using the 40%-60% split and experiment is excellent, within the approximations made, a fact that lends further credence to this more recently established distribution of the GaAs-$Al_{1-x}Ga_xAs$ energy-gap discontinuity.

ACKNOWLEDGMENTS

This work was supported in part by the National Science Foundation Grant No. DMR-80-18440.

*Present address: Naval Research Laboratory, Code 6877, Washington, D.C. 20375-5000.

[1]R. Dingle, in *Festkörperprobleme*, Vol. 15 of *(Advances in Solid State Physics)*, edited by H. J. Queisser (Pergamon/Vieweg, Braunschweig, 1975), p. 21.

[2]R. C. Miller, D. A. Kleinman, W. T. Tsang, and A. C. Gossard, Phys. Rev. B **24**, 1134 (1981).

[3]G. Bastard, E. E. Mendez, L. L. Chang, and L. Esaki, Phys. Rev. B **26**, 26 (1982).

[4]R. L. Greene, K. K. Bajaj, and D. E. Phelps, Phys. Rev. B **29**, 1807 (1984).

[5]U. Fano, Phys. Rev. **124**, 1866 (1961).

[6]B. Velicky and J. Sak, Phys. Status Solidi **16**, 147 (1966).

[7]R. C. Miller, D. A. Kleinman, and A. C. Gossard, Phys. Rev. B **29**, 7085 (1984).

[8]H. C. Casey and M. B. Panish, in *Heterostructure Lasers, Part A* (Academic, New York, 1978).

[9]D. J. BenDaniels and C. B. Duke, Phys. Rev. **152**, 683 (1966).

[10]J. M. Luttinger, Phys. Rev. **102**, 1030 (1956).

[11]D. A. Broido and L. J. Sham, Phys. Rev. B **31**, 888 (1985).

[12]K. Hess, D. Bimberg, N. O. Lipari, J. U. Fishbach, and M. Altarelli, in *Proceedings of the 13th International Conference*

on the Physics of Semiconductors, Rome, 1976, edited by F. G. Fumi (North-Holland, Amsterdam, 1976), p. 142.

[13]S.-R. Eric Yang, D. A. Broido, and L. J. Sham, Phys. Rev. B **32**, 6630 (1985).

[14]L. J. Sham and T. M. Rice, Phys. Rev. **144**, 708 (1966).

[15]T. Ando, A. B. Fowler, and F. Stern, Rev. Mod. Phys. **54**, 437 (1982).

[16]C. T. H. Baker, in *Numerical Treatment of Integral Equations* (Clarendon, New York, 1977).